Remote Sensing and Evapotranspiration Mapping: State of the Art

W.W. Immerzeel
P. Droogers
A. Gieske

NIVR
Nederlands Instituut voor Vliegtuigontwikkeling en Ruimtevaart
Netherlands Agency for Aerospace Programmes

Research paper no. 1

IWMI
International
Water Management
Institute

Future Water
Science for Solutions

P.O. Box 35

2600 AA Delft

The Netherlands

Kluyverweg 1

2629 HS Delft

The Netherlands

Tel. +31 (0)15 278 80 25

Fax +31 (0)15 262 30 96

Email info@nivr.nl

www.nivr.nl

NATIONAL USER SUPPORT PROGRAMME (NUSP)
2001-2005

http://www.ao-go.nivr.nl

The National User Support Programme 2001-2005 (NUSP) is executed by the Netherlands Agency for Aerospace Programmes (NIVR) and the Space Research Organization of the Netherlands (SRON). The NUSP is financed from the national space budget. The NUSP subsidy arrangement contributes to the development of new applications and policy-supporting research, institutional use and use by private companies.

The objectives of the NUSP are:

- To support those in the Netherlands, who are users of information from existing and future European and non-European earth observation systems in the development of new applications for scientific research, industrial and policy research and operational use;

- To stimulate the (inter)national service market based on space-based derived operational geo-information products by means of strengthening the position of the Dutch private service sector;

- To assist in the development of a national Geo-spatial data and information infrastructure, in association with European and non-European infrastructures, based on Dutch user needs;

- To supply information to the general public on national and international space-based geo-information applications, new developments and scientific research results.

Remote Sensing and Evapotranspiration Mapping: State of the Art

Authors: W. Immerzeel (FutureWater)

             P. Droogers (FutureWater)

             A. Gieske (ITC)

Preface

This report contributes to a research project undertaken by FutureWater entitled: "Remotely Sensed based hydrological model calibration for basin scale water resources planning: embedding case for Krishna Basin, India" (GO-2005/025). This project is financially supported by NIVR (Nederlands Instituut voor Vliegtuigontwikkeling en Ruimtevaart) in the context of "Tijdelijke subsidieregeling Nationaal Programma Gebruikers Ondersteuning (GO).

The report describes the state of the art in Remote Sensing and evapotranspiration mapping

FutureWater
Generaal Foulkesweg 28
6703 BS Wageningen
tel: 0317 460050
email: info@futurewater.nl

Table of contents

1   Introduction

Evapotranspiration is a collective term that includes water discharged to the atmosphere as a result of evaporation from the soil and surface-water bodies and as a result of plant transpiration. Evapotranspiration is an important component of the water cycle. Figure 1 shows an overview of the global water cycle. It shows that over land approximately 75% of the total precipitation is evapotranspired (70,000 km^3/year) by the plants and soil. Given a total land surface area of 148,940,000 km^2 this roughly equals 470 mm/year. Over the oceans this amount is even much higher (425,000 km^3). Evapotranspiration, also referred to as a latent heat flux when expressed as energy flux, is the most important mechanism of energy and mass exchange between the hydrosphere, biosphere and atmosphere. Evapotranspiration is a function of water and energy availability, near-surface atmospheric conditions (e.g. air temperature, relative humidity and wind-speed) and the control of transpiration by plants.
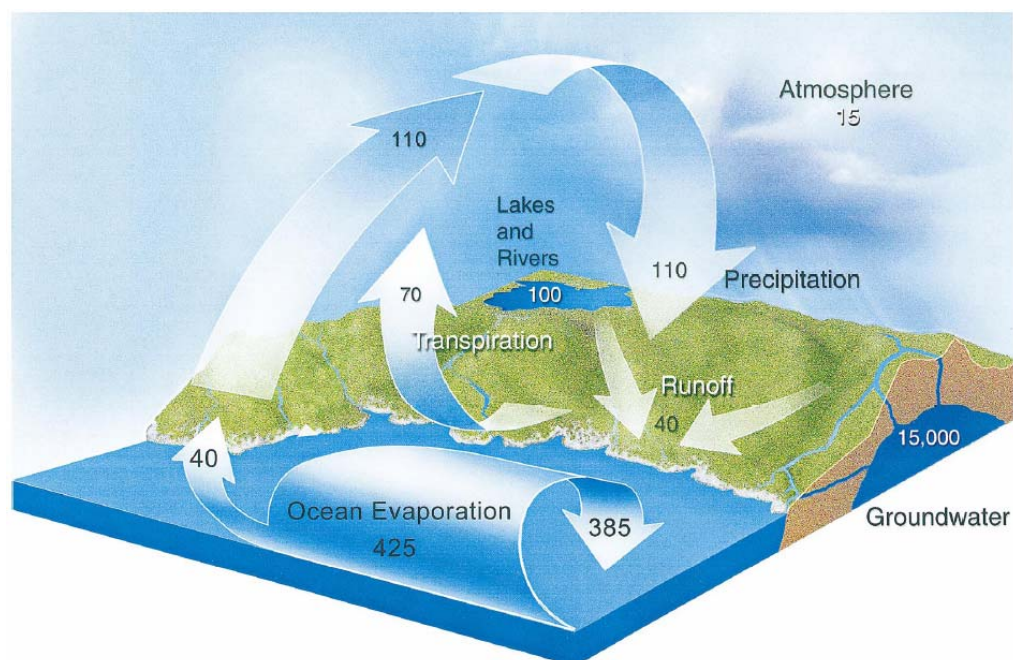

Figure 1: Global hydrological cycle in 1000 km^3/year. Numbers in white are pools and numbers in black are fluxes (Jackson et al., 2001).

Calculation of turbulent atmospheric fluxes is a complex task given the chaotic behaviour of turbulence and the many variables involved. Being able to accurately predict spatially explicit actual evapotranspiration across large heterogeneous landscapes is an even more daunting task for which Remote Sensing has proven to be the only appropriate instrument. In this report we first summarize the turbulence theory underlying most methods, and then we provide a brief overview of a number of quantitative methods to measure evapotranspiration. First methods based on estimating evapotranspiration using field measurements are discussed followed by a more in-depth overview of Remote Sensing methods.

2 Physical background of turbulent transport[1]

2.1 Introduction

Atmospheric transport of water vapor close to the surface takes place mainly by diffusive processes, while further away the transport is dominated by turbulent transfer due to increasing wind speed and buoyancy effects. The theory of these physical transport processes was extensively described by, for example, Brutsaert (1982), Panofsky and Dutton (1984) and Garratt (1992). Although a complete account of the theoretical development is clearly beyond the scope of this chapter, a short outline is indispensable for an understanding of the parameterizations of current operational applications. Therefore a summary description is given of the atmospheric boundary layers and type of surfaces involved. This is followed by a discussion of the mean logarithmic wind profile, shear stress and friction velocity. The approach is then extended to include similar expressions for specific humidity and temperature: the so-called scalar quantities. The theory for CO_2 transport and radioactive deposition follows along the same lines, but is not further discussed here. It is necessary to discuss the roughness parameters for momentum, heat and water vapor transport in some detail because these appear in the Penman-Monteith formulation for reference crop evapotranspiration and because their determination forms a major bottleneck in the determination of land surface fluxes. Finally, the effects of stable and unstable atmospheric conditions are incorporated in the equations.

2.2 The Atmospheric Boundary Layer

In the atmosphere the largest changes in wind, temperature and humidity take place near the surface. For this reason the air near the surface may be regarded as a boundary layer for momentum, heat and mass transport. In this context one usually refers to the Atmospheric Boundary Layer, which is subdivided as follows (Figure 2)

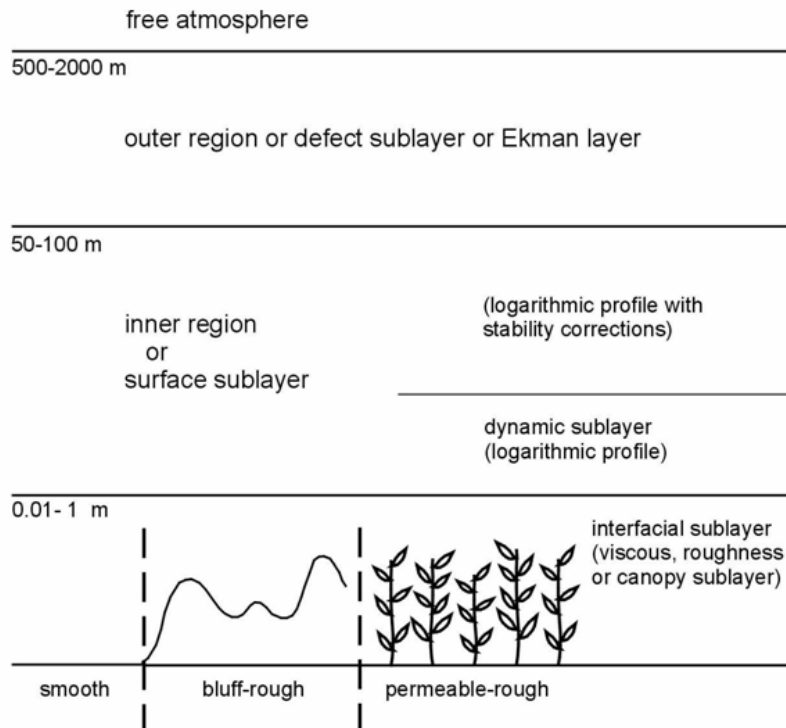[1] Text provided in this chapter is extracted from Gieske (2003)

Figure 2 Definition sketch showing simplified sublayers of the Atmospheric Boundary layer after Brutsaert (1982). The heights in m indicate the variable heights of the boundaries (not to scale)

The flow in the "free" atmosphere above the boundary layer (ABL) is that of a free stream, affected mainly by the pressure field and Earth rotation, but very little by friction with the surface. The top of the Atmospheric Boundary Layer varies between 500 and 2000 m. However, this strongly depends on atmospheric conditions and on whether it is day or night. For example, over deserts under strong surface heating the thickness of the ABL may be 5km or more. Over open oceans the ABL thickness is usually less than over land. The top of the ABL is in convective conditions often well defined by a stable inversion layer.

The ABL is subdivided into an inner and outer region. The transition between inner and outer region is gradual rather than abrupt. The outer region is also called defect sublayer or Ekman layer while the flow in this region is nearly independent of the surface characteristics and largely determined by the free stream velocity. The flow in the inner region or surface sublayer is characterized by the nature of the Earth's surface. The lower part of the inner region is called the dynamic sublayer.

Finally below the dynamic sublayer and directly above the surface lies the interfacial sublayer, where the turbulence is strongly affected by the roughness of the surface elements. In this layer molecular diffusivities can no longer be neglected in the description of water vapour and heat transport mechanisms. In the case of smooth flow this layer is often called the viscous sublayer, while over a rough surface it may be referred to as roughness sublayer (Brutsaert, 1982). Finally over vegetation many complications arise depending on foliage density and canopy depth, and in this case the layer is often called canopy sublayer.

2.3   *Logarithmic wind profile*

When the wind blows across a surface, it is observed that the wind speed is a function of the height above the surface. The wind speed is zero at the surface because of frictional effects of the air with the surface and increases steadily with increasing height. Thus the air momentum becomes less with decreasing height. The downward transport of momentum is caused mainly by turbulent eddies, and the effectiveness of this transport mechanism is described by the friction velocity u_* (ms^{-1}) which by definition (Brutsaert, 1982) is related to shear stress τ_0 (N m^{-2}) as

$$u_* = \sqrt{\frac{\tau_0}{\rho}}$$

Eq. 1

Where ρ is the average air density (kg m^{-3}). The shear stress τ_0 is generally taken as constant for the inner region of the ABL. It appears that this is a sufficiently accurate assumption for heights of up to 100 m above the surface.

The nature of the wind speed change with elevation has been investigated extensively since the 1920s and was first introduced in meteorology by Prandtl (1932). The results are usually written as

$$\frac{u_*}{z\left(d\bar{u}/dz\right)} = k$$

Eq. 2

Where $\bar{u}$ is the average wind speed (m s^{-1}) and z is the elevation above the surface (m). Experimentally it was found that the left hand side Eq. 2 is constant k, which is referred to as von Kárman's constant and is usually taken as 0.41. The logarithmic wind profile equation follows immediately from integration of Eq. 2.

$$\bar{u}_2 - \bar{u}_1 = \frac{u_*}{k}\ln\left(\frac{z_2}{z_1}\right)$$

Eq. 3

where the subscripts refer to two levels in the dynamic sublayer. The level at which u_1 becomes zero is called the momentum roughness length z_{om} (m) and Eq. 3 is then written as

$$\bar{u} = \frac{u_*}{k}\ln\left(\frac{z}{z_{om}}\right)$$

Eq. 4

The momentum roughness length may be visualized graphically as the zero velocity intercept of the straight line resulting from a semi-logarithmic plot of mean wind speed versus elevation (Figure 3).
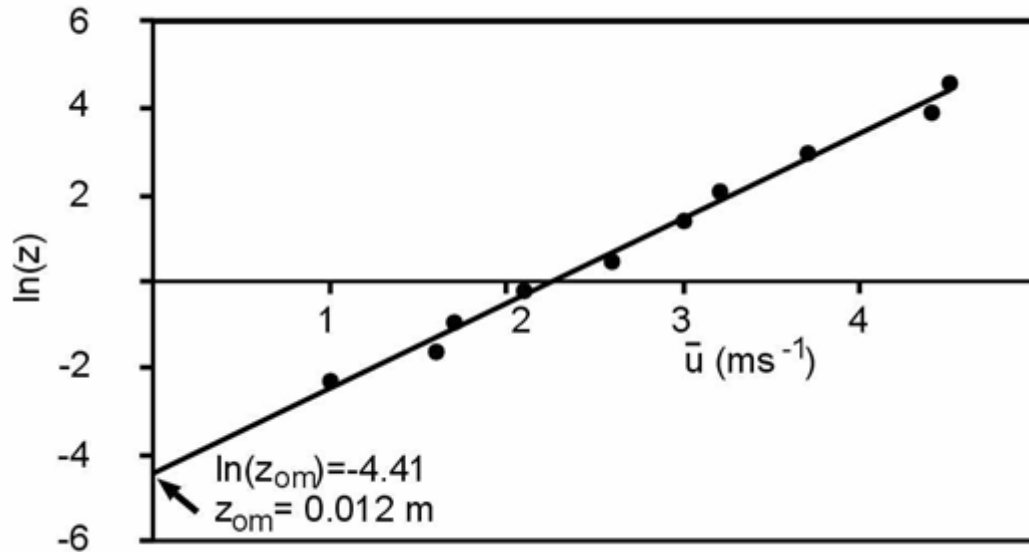
Figure 3 Example plot of mean wind speed against ln(z). The intercept with the vertical axis leads to $z_{om} = 0.012$ m.

In the case of rough surfaces there is some ambiguity concerning the reference level z=0 as used in Eq. 2- Eq. 4. For very sparsely spaced roughness elements on a flat plane this level can be taken at the level of the plane. However, the denser these roughness elements become, the closer to the top the zero level has to be placed. In practice this difficulty is solved by introducing a displacement distance d (m). The reference level (z=0) is at the base of the roughness elements, and the wind speed is zero at $z=d+z_{om}$. The variable (z-d) is then used instead of z Eq. 2- Eq. 4. For example Eq. 4 becomes

$$\overline{u} = \frac{u_*}{k} \ln\left(\frac{z-d}{z_{om}}\right)$$

Eq. 5

Figure 4 illustrates the situation for a crop of height h (m). The displacement height d is then usually taken as 0.7 or 0.8 times h. The wind speed becomes zero at $d+z_{om}$.

2.4 Mean specific humidity and temperature profiles

The approach that led to Eq. 2- Eq. 5 can now be used to derive expressions for the mean specific humidity and temperature profile. In the dynamic sub-layer these are passive admixtures of the air and they do not affect the dynamics of the flow. As opposed to wind speed and momentum, which are vectors, humidity and temperature are scalar quantities. The same holds for CO_2 transport.

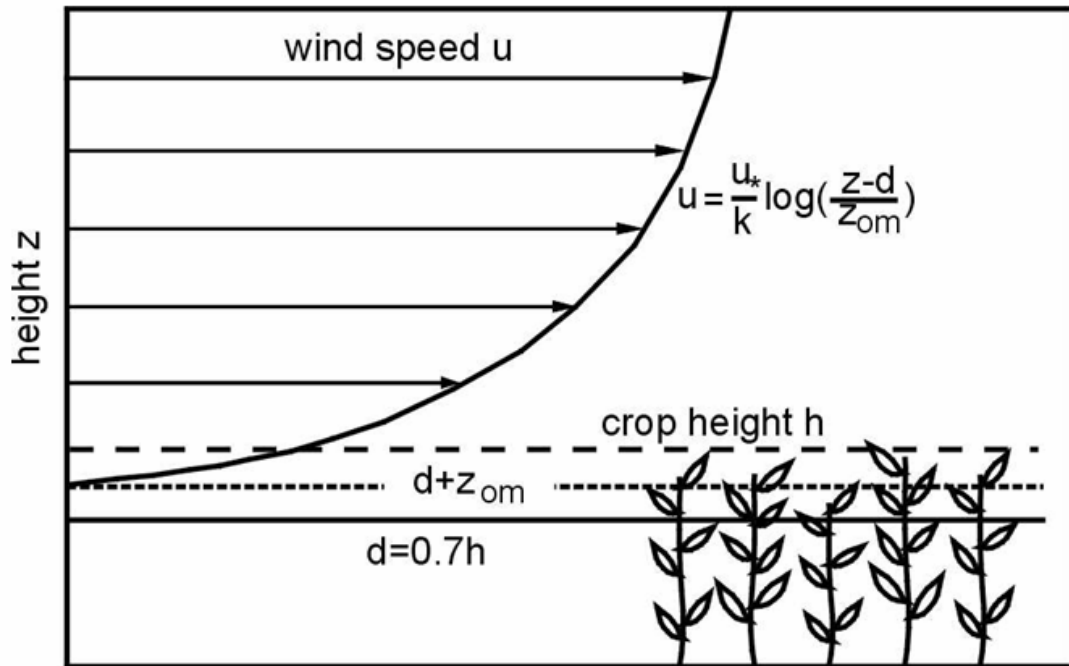**FutureWater** Science for Solutions

Figure 4: Vertical distribution of wind speed over a vegetated surface of height h. The profile follows the logarithmic distribution of Eq. 4 . The zero plane displacement d is about 0.7h. The wind speed becomes zero at d+z$_{om}$

Through application of the same principles as were used in establishing Eq. 2 (Reynolds analogy) the gradient of the specific humidity q(-) can be related to the water vapor flux E (kg m^{-2} s^{-1}) by

$$\frac{E}{\rho u_* (z-d)(d\bar{q}/dz)} = -k_v$$

Eq. 6

where $k_v=a_v k$ is von Kármán's constant for water vapor. It has been found that a_v is usually close to unity, and the difference between k_v and k will therefore be ignored. Integrating (6) between two arbitrary levels z_1 and z_2 within the dynamic sublayer yields

$$\bar{q}_1 - \bar{q}_2 = \frac{E}{k\rho u_*}\ln\left(\frac{z_2-d}{z_1-d}\right)$$

Eq. 7

If q_s is the value of q at the surface, the profile can also be written as (see Eq. 5)

$$\bar{q}_s - \bar{q} = \frac{E}{k\rho u_*}\ln\left(\frac{z-d}{z_{0v}}\right)$$

Eq. 8

where z_{0v} (m) is the water vapor roughness length. The integration constant z_{0v} can be visualized as the level above the displacement distance d where the mean specific humidity q would assume its surface value if the logarithmic profile were extrapolated downward. It should be noted that z_{0v} has no real physical meaning because close to the surface diffusive processes prevail and the assumptions underlying Eq. 6-Eq. 8 with regard to turbulent transport are no longer valid.

Similar procedures for temperature profiles are followed, with the exception that potential temperature θ (K) is used rather than air temperature T (K)

$$\theta = T + \Gamma z \qquad\qquad Eq.\ 9$$

where Γ is the dry adiabatic lapse rate (0.01 K m^{-1}). Because of its low value the difference between Γ and T can be ignored in many applications.

The expression for the temperature profile is similar to the relation for specific humidity (Eq. 7)

$$\overline{\theta}_1 - \overline{\theta}_2 = \frac{H}{k\rho\, c_p u_*} \ln\left(\frac{z_2 - d}{z_1 - d}\right) \qquad\qquad Eq.\ 10$$

or

$$\overline{\theta}_s - \overline{\theta} = \frac{H}{k\rho\, c_p u_*} \ln\left(\frac{z - d}{z_{oh}}\right) \qquad\qquad Eq.\ 11$$

where C_p is the specific heat at constant pressure (J kg^{-1} K^{-1}), H (W m^{-2}) is the sensible heat flux as a result of the temperature differences in the profile and where z_{oh} (m) is the roughness length for sensible heat. The same comments hold for z_{oh} as for z_{ov}. Close to the surface diffusive rather than turbulent processes prevail and care should be taken in attaching a physical meaning to z_{oh}. The determination of a representative surface temperature θ_s or T_s is a difficult practical problem, especially with infrared sensor techniques.

2.5   Stability corrections in the surface sublayer

Above the dynamic sublayer the stability of the atmosphere needs to be considered, that is the effect from the buoyancy resulting from the effective vertical density gradient. The common way to include the stability corrections is through introduction of a variable L (m), the stability length, as was first proposed by Monin and Obukhov (1954). This variable was defined by similarity theory through dimensional analysis of the variables involved

$$L = \frac{- u_*^{3} \rho\, c_p T_a}{kgH} \qquad\qquad Eq.\ 12$$

Where g is the acceleration of gravity (9.8 m s^{-2}) and T_a is the air temperature (K).

A more precise formulation is

$$L = \frac{-u_*^3 \rho}{kg\left[\left(\dfrac{H}{c_p T_a}\right) + 0.61E\right]}$$

Eq. 13

However, Eq. 12 is often used instead of Eq. 13. After introducing the dimensionless variable ζ as

$$\zeta = \frac{z - d}{L}$$

Eq. 14

the expressions for wind speed, water vapor and temperature become

$$\frac{k(z - d)}{u_*}\frac{du}{dz} = \phi_{sm}(\zeta)$$

Eq. 15

$$-\frac{k\rho u_*(z - d)}{E}\frac{dq}{dz} = \phi_{sv}(\zeta)$$

Eq. 16

$$-\frac{k\rho c_p u_*(z - d)}{H}\frac{d\theta}{dz} = \phi_{sh}(\zeta)$$

Eq. 17

After integrating Eq. 15, Eq. 16 and Eq. 17 the following set of equations is obtained

$$u_2 - u_1 = \frac{u_*}{k}\left[\ln\left(\frac{\zeta_2}{\zeta_1}\right) - \psi_{sm}(\zeta_2) + \psi_{sm}(\zeta_1)\right]$$

Eq. 18

$$q_1 - q_2 = \frac{E}{k\rho u_*}\left[\ln\left(\frac{\zeta_2}{\zeta_1}\right) - \psi_{sv}(\zeta_2) + \psi_{sv}(\zeta_1)\right]$$

Eq. 19

$$\theta_1 - \theta_2 = \frac{H}{k\rho c_p u_*}\left[\ln\left(\frac{\zeta_2}{\zeta_1}\right) - \psi_{sh}(\zeta_2) + \psi_{sh}(\zeta_1)\right]$$

Eq. 20

Note that the overbars in these equations have been left out for convenience. Averaging is implied in the remainder of this chapter. The ψ functions are defined as

$$\psi = \int \left(\frac{1 - \phi(\zeta)}{\zeta} \right) d\zeta \qquad \text{Eq. 21}$$

Much experimental work has been done to determine the proper ϕ and ψ functions for different meteorological conditions and usually a distinction is made between stable conditions, prevailing at night, and unstable conditions, arising from the strongly convective conditions normally encountered during the day. Under unstable conditions heat flow is away from the surface while under stable circumstances heat flow is towards the surface. Under neutral conditions in the dynamic sublayer, the ϕ functions are equal to unity, and the equations reduce to those of the mean logarithmic profiles discussed above.

Unstable conditions

Several experimentally determined forms of the functions ϕ exist and one common choice is

$$\phi_{sv} = \phi_{sh} = \phi_{sm}{}^2 = (1 - 16\zeta)^{-1/2} \qquad \text{Eq. 22}$$

where the following ψ-functions are found when using Eq. 22 in the evaluation of Eq. 21.

$$\psi_{sm} = 2\ln\left[\frac{(1+x)}{2} \right] + \ln\left[\frac{(1+x^2)}{2} \right] - 2\arctan(x) + \pi/2 \qquad \text{Eq. 23}$$

$$\psi_{sv}(\zeta) = \psi_{sh}(\zeta) = 2\ln\left[\frac{(1+x^2)}{2} \right] \qquad \text{Eq. 24}$$

and x is defined as

$$x = (1 - 16\zeta)^{1/4} \qquad \text{Eq. 25}$$

Stable conditions

Some discrepancies exist between various experimental results, and many forms of ϕ are suggested in the literature. It appears, however, that fluxes are small under stable conditions and the exact form of these relations is not critical. For practical work it was suggested already by Brutsaert (1982) to use

$$\phi_{sv} = \phi_{sm} = \phi_{sh} = 1 + 5\zeta \qquad \text{for } 0 < \zeta < 1$$

$$\text{Eq. 26}$$

$$\phi_{sv} = \phi_{sm} = \phi_{sh} = 6 \qquad \text{for } \zeta > 1$$

FutureWater Science for Solutions

2.6 *Applications*

Suppose that measurements of wind are taken at a level z_1, and measurements of temperature at levels z_1 and at the surface (z-d=0). Suppose further that neutral conditions prevail and therefore stability corrections do not have to be made. Then Eq. 5 and Eq. 11 allow determination of u_* and H. First u_* is determined from Eq. 5

$$u_* = \frac{ku}{\ln\left(\dfrac{z_1 - d}{z_{om}}\right)}$$

Eq. 27

Then H is determined by substitution of Eq. 27 into Eq. 11 as

$$H = \frac{k^2 \rho\, c_p\, u\, (T_s - T_1)}{\ln\left(\dfrac{z_1 - d}{z_{om}}\right)\ln\left(\dfrac{z_1 - d}{z_{oh}}\right)}$$

Eq. 28

This can be done provided of course values for z_{om}, z_{oh} and d have been determined beforehand. The surface roughness for ordinary farm and grassland is usually much smaller than 0.1 m. and may range up to 0.5 m. for dense forests. The values for z_{oh} show much more variability (see e.g. Sugita and Brutsaert, 1990 and Verhoef et al., 1997). For reference crop evapotranspiration (Allen et al., 1994) z_{oh} is normally taken as 0.1 z_{om}. The logarithmic ratio of the roughness lengths for momentum and heat is defined as kB^{-1}

$$kB^{-1} = \ln\left(\frac{z_{om}}{z_{oh}}\right)$$

Eq. 29

For a ratio of 10 this gives kB^{-1}=2.3. Especially in semi-arid areas much higher values may be found and, moreover, these show distinct diurnal and seasonal variability. The interpretation of z_{oh} still appears unclear in many field situations.

Eq. 28 is used in the Penman-Monteith formulation (Allen et al., 1998) of reference crop evapotranspiration through the definition of sensible heat H as

$$H = \rho\, c_p\, \frac{T_s - T_z}{r_{ah}}$$

Eq. 30

where T_z (K) is the air temperature at height z, and r_{ah} (s m^{-1}) is defined as the aerodynamic resistance to heat transport. Comparing Eq. 28 with Eq. 30 this leads to

$$r_{ah} = \frac{1}{k^2 u} \left[\ln\left(\frac{z-d}{z_{om}}\right) \right]\left[\ln\left(\frac{z-d}{z_{oh}}\right) \right]$$

Eq. 31

If the stability corrections ψ are used in the formulation of the profile equations, then Eq. 28 is changed to

$$H = \frac{k^2 \rho\, c_p\, u\left(T_s - T_z\right)}{\left[\ln\left(\frac{z-d}{z_{om}}\right) - \psi_{sm}\left(\frac{z-d}{L}\right) \right]\left[\ln\left(\frac{z-d}{z_{oh}}\right) - \psi_{sh}\left(\frac{z-d}{L}\right) \right]}$$

Eq. 32

Since L depends on H through Eq. 13, Eq. 32 is an implicit equation in H, which is usually solved by iteration.

Note that the water vapor flux E can in principle be solved in the same way as the sensible heat flux H, for example, by combining Eq. 8 and Eq. 5 for neutral atmospheric conditions.

FutureWater Science for Solutions

3   Methods based on field measurements

There are many methods developed to measure actual evapotranspiration. The following methods can be distinguished: pan evaporation method, lysimeters, flux profile measurements, the FAO56 method, the Bowen ratio, eddy-correlation, and scintillometer measurements. The most important methods will be discussed in this chapter. For this project these methods are not suitable because they are all, with the exception of the scintillometer, point methods which do not provide spatial patterns of actual evapotranspiration. The discussion of the principles used is however very relevant.

Most methods used to estimate the latent heat flux are based on a combination of the energy balance approach, flux methods and the Monin-Obukhov similarity theory (Monin and Obukhov, 1954). The energy balance is given by:

$$Q^* = G_0 + H + L_v E$$

<div align="right">Eq. 33</div>

Where Q^* (W m^{-2}) is the net radiation, H (W m^{-2}) is the sensible heat flux and $L_v E$ (W m^{-2}) is the latent heat flux (L_v (J kg^{-1}) is the latent heat of vaporization and E (kg m^{-2} s^{-1}) is the actual evapotranspiration) and G_0 is the soil heat flux (W m^{-2}). The net radiation produced by the sun is shared between the two atmospheric convective fluxes and the soil heat flux. Commonly used flux profile relations based on layer resistance schemes have been derived for H and $L_v E$:

$$H = \rho c_p \frac{T_0 - T}{r_a}$$

<div align="right">Eq. 34</div>

and

$$L_v E = \frac{\rho c_p}{\gamma} \frac{e_0 - e}{r_a + r_s}$$

<div align="right">Eq. 35</div>

Where ρ (kg m^{-3}) and c_p (J kg^{-1} K^{-1}) are the density and specific heat of air at constant pressure, γ is the psychometric constant, T_0 (K) is the temperature at the earth surface, T (K) is the air temperature at an height of 2 meter, e_0 (Pa) is the surface vapor pressure, e (Pa) is the vapor pressure at a height of 2 meter, r_a (s m^{-1}) is the aerodynamic resistance, r_s (s m^{-1}) is the surface resistance. These flux profiles assume that vertical fluxes of momentum, heat and water can be quantified by gradients in wind, temperature and vapor pressure respectively. The aerodynamic resistance is derived using the Monin-Obukhov similarity theory as described above.

By assuming that over a water surface the saturated vapor pressure (e_w (Pa)) is equal to the actual vapor pressure the solution of this set of equations leads to the famous Penman-Monteith equation (Penman (1948), Monteith (1965)).

$$L_v E = \frac{s(Q^* - G) + \frac{\rho c_p}{r_a}(e_w(T) - e)}{s + \gamma(1 + \frac{r_s}{r_a})}$$

Eq. 36

with s being the slope of the saturation vapor pressure temperature relationship and $e_w(T)$ the saturated . The determination of instantaneous aerodynamic and surface resistances is complex. The atmospheric resistance depends on the atmospheric stability, zero displacement heights and, roughness lengths for heat transfer and wind speed. The surface resistance describes the resistance of vapor flow through the transpiring crop and evaporating soil surface. The surface resistance is depending on the soil cover, the type of crop, air temperature, incident solar radiation, moisture deficit and available soil moisture.

3.1   FAO 56 methodology

An operational application of the above equations is the method described in FAO's Irrigation and Drainage paper no. 56 (Allen et al., 1998). The FAO 56 method is applied in numerous countries by water managers and irrigation engineers. The FAO 56 methodology calculates reference evaporation (ET_0) using the Penman-Monteith equation for a hypothetical reference surface defined as " a hypothetical reference crop with an assumed crop height of 0.12 m, a fixed surface resistance of 70 s m^{-1} and an albedo of 0.23. The method uses measured meteorological data as inputs (air temperature, humidity, radiation and wind speed). The following equations and assumptions are used in deriving the variables of the Penman-Monteith equation.

- The net radiation is calculated by:

$$Q^* = (1 - \alpha_{surface})Q_{sw} + \varepsilon_{surface}Q_{lw} - \varepsilon_s \sigma T_{surface}^4$$

Eq. 37

  Where $\alpha_{surface}$ is the surface albedo, Q_{sw} (W m^{-2}) is the incident shortwave solar radiation, $\varepsilon_{surface}$ is the surface emissivity, Q_{lw} (W m^{-2}) is the incident long wave radiation, σ is the Stefan-Boltzmann constant (5.67 10^{-8} W m^{-2} K^{-4}) and $T_{surface}$ (K) is the surface temperature.

- The soil heat flux is calculated by

$$G = C \frac{T_i + T_{i-1}}{\Delta t} \Delta z$$

Eq. 38

FutureWater Science for Solutions

Where C is the soil heat capacity (J m^{-3} K), T_i (K) is the air temperature at time i, T_{i-1} (K) is the air temperature at time i-1, Δt (s) is the length of the time interval, Δz (m) is the effective soil depth.

- The variables $e_w(T)$, e and s are calculated using air temperature and relative humidity measurements.
- The surface resistance is a function of the Leaf Area Index and for the reference crop equal to 70 m s^{-1}.
- The aerodynamic resistance, given by the Monin-Obhukov similarity theory (Monin, 1971, Obukhov, 1946) is given by:

$$ r_a = \frac{\ln\left[\dfrac{z_m - d}{z_{0m}}\right] \ln\left[\dfrac{z_h - d}{z_{0h}}\right]}{k^2 u_z} \qquad \text{Eq. 39} $$

Where z_m (m) is the height of the wind measurement, z_{0m} (m) is the roughness length for momentum transfer, z_{oh} (m) is the roughness length for heat and vapor transfer, z_h (m) is the height of the humidity measurement, d (m) is the zero plane displacement height, k is the Von Karman constant (0.4) and u_z (m s^{-1}) is the wind speed at height z_m. For the reference crop the aerodynamic resistance can be reduced to:

$$ r_a = \frac{208}{u_2} \qquad \text{Eq. 40} $$

The reference evapotranspiration is only affected by climatic parameters and can be computed by weather variables only and is valid for the hypothetical reference crop under well watered conditions. The next step in the FAO procedure is to determine the crop evapotranspiration under standard condition for a specific crop (ET$_c$); disease free, well fertilized, grown in large fields, under optimum soil water conditions. The only difference between the ET$_c$ and ET$_0$ is caused by differences between leaf anatomy, stomata characteristics, aerodynamic properties and albedo. ET$_c$ is given by

$$ ET_c = K_c ET_0 \qquad \text{Eq. 41} $$

Where K_c is the crop coefficient. The crop coefficient varies in time and depends on the crop growth stage and the climatic conditions or management operations (e.g. irrigation) during the stage. If ET_c

Is required on a daily basis it is necessary to split the crop coefficient into a separate plant transpiration and soil evaporation coefficient. ET_c is also referred to as potential evapotranspiration.

In practice plants usually are under environmental stress (e.g. soil water stress) which causes the actual evapotranspiration to be lower than the potential evapotranspiration. The FAO56 methodology takes environmental stress into account by introducing an environmental stress factor. The actual evapotranspiration ($ET_{c\ adj}$) is given by:

$$ET_c = K_s K_c ET_0 \qquad\qquad Eq.\ 42$$

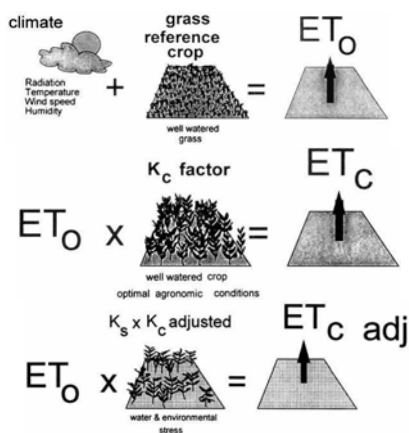Where K_s is the environmental stress factor. An overview is given in Figure 1.

Figure 5: Reference evepotranspiration (ET_0), crop evapotranspiration under standard conditions (ET_c) and non-standard condition ($ET_{c\ adj}$), (Allen et al., 1998)

The FAO56 methodology is relatively straightforward and therefore applied in many countries across the world; however there is one disadvantage. The calculated reference evapotranspiration is based on meteorological information for a specific station and is therefore not known spatially distributed. Sensitive variables in the potential evapotranspiration calculation, such as the surface temperature, radiation, wind speed and relative humidity are all highly variable in space. Surface and aerodynamic resistances are also varying in space and depend on land use and wind speed. The calculation of actual evapotranspiration depends on a crop factor, which depends on the development stage, type and variety of the crop and the soil cover, and on an environmental stress factor which is also location specific. In other words the methodology is not suitable to estimate spatially distributed evapotranspiration. Remote Sensing data with increased spatial and temporal resolution is therefore a useful tool to provide information on evapotranspiration on various temporal and spatial scales.

The FAO56 method estimates evapotranspiration on the basis of meteorological input data at a specific location.

3.2   Bowen Ratio

The Bowen ratio method (Bowen, 1926) is also based on the energy balance. The Bowen ratio (β) is defined as the quotient of sensible and latent heat flux:

$$\beta = \frac{H}{L_v E} = \frac{c_p \Delta\overline{\theta}/r_{ah}}{L_v \Delta\overline{q}/r_{av}} = \frac{c_p \Delta\overline{\theta}}{L_v \Delta\overline{q}}$$

Eq. 43

Where $\Delta\overline{\theta}$ (K) is the average difference in potential temperature between two heights, $\Delta\overline{q}$ is the average difference in specific humidity, and r_{ah} and r_{av} are the aerodynamic resistances to heat and vapor transport respectively. Since the stability functions for heat and vapor are similar Bowen assumed the aerodynamic resistances to heat and vapor transport are also equal. The Bowen ration can therefore be determined by measurements of temperature and specific humidity at two different heights above the surface.

By combining the Bowen ratio with energy balance the latent heat flux can be determined as follows:

$$L_v E = \frac{Q^* - G}{1 + \beta}$$

Eq. 44

The net radiation can be determined by a net radiometer and the soil heat flux by soil heat flux plates.

The advantage of the Bowen Ratio method is the ability to measure actual evapotranspiration and that it eliminates wind and turbulent transfer coefficients. The disadvantage is the need for fragile sensors and data loggers, the need for a upwind fetch and the numerical instability when the Bowen ration approaches -1.

3.3   Eddy correlation method

The eddy correlation method is based on Reynolds decomposition, which forms the basis of the turbulence theory. The value of a quantity A can be written as:

$$A = \overline{A} + A^{'}$$

Eq. 45

Where A s the value of quantity A at time t, $\overline{A}$ is the average value of A and $A^{'}$ is the turbulent deviation of the average, generally referred to as the fluctuation part.

Evaporation (kg m^{-2}) can be written as the average product over a certain time interval of the vertical component of the wind speed w (m s^{-1}), the air density ρ (kg m^{-3}) and the specific air humidity q :

$$E = \overline{w\rho\, q}$$

<div align="right">Eq. 46</div>

Using Reynolds decomposition and some simplification this can be rewritten to:

$$E = \overline{\rho}\,\overline{w'q'}$$

<div align="right">Eq. 47</div>

This means that the evapotranspiration can be calculated by the covariance of the vertical wind speed and specific humidity and the air density. This requires high frequency sensors which can measure the wind speed and specific humidity around 10 times per second. This can be achieved by using sonic anemometers which measure the different directional components of the wind speed and the sonic temperature and a Licor sensor which measures H_2O concentrations in the air.
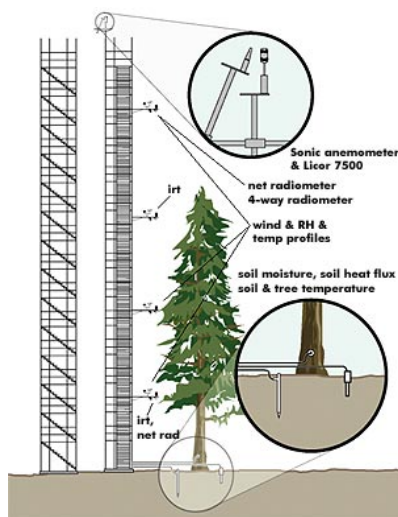

Figure 6: Typical set-up of an eddy correlation tower

The advantage of the eddy correlation method is that it directly measures atmospheric turbulence, but skilled staff, complex instrumentation and adequate upwind fetch is required.

3.4 Scintillometer

A methodology which estimates evapotranspiration at a scale of several kilometers is the scintillation method. The scintillation method is also based on the Monin-Obhukov similarity theory and it is applicable over distances as long as 5 km (De Bruin et al., 1995). A large scintillometer is a device which consists of a transmitter and a receiver and measures the turbulent intensity of the refraction index of air. Variations in the refraction index are caused by fluctuations in temperature and humidity, which can be used to calculate the latent heat flux using the flux-profile relationships and the similarity theory. The scintillation method is an intermediate between in situ field measurements and large area Remote Sensing estimates. Figure 7 shows the operational principle of a scintillometer. Light from a Light Emitting Diode (LED) is bundled in a parallel beam and modulated by a 7KHz oscillator. The light

FutureWater Science for Solutions

signal is amplified by a receiver and the signal is representative of changes in the refractive index of the atmosphere, which is in its turn the result of the sensible heat flux.
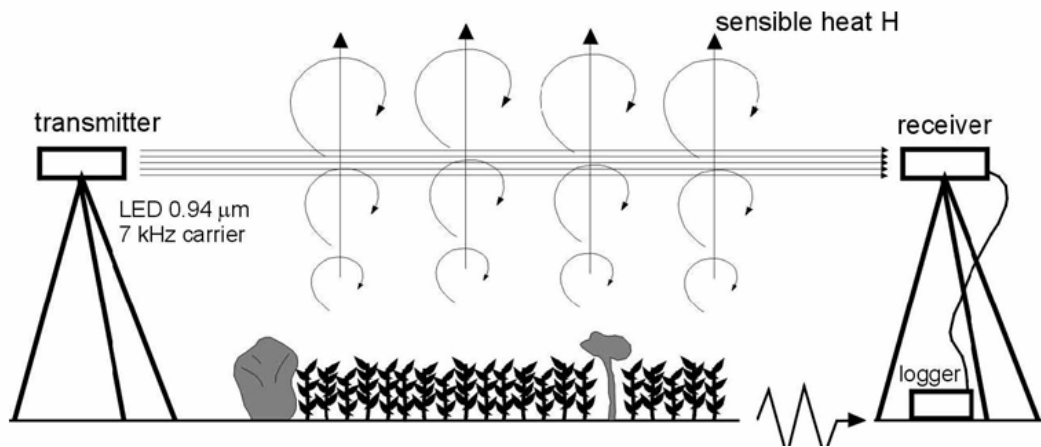

Figure 7: Operational principle of a scintillometer

The refractive index structure parameter (C_n) is related to the temperature structure parameter (C_T) as

$$C_T = 10^6 \left(\frac{C_n T^2}{0.78p} \right) \cdot \left(1 + \frac{0.03}{\beta} \right)$$

Eq. 48

Where p is the atmospheric pressure (bar), T is the temperature (K) and β is the Bowen ratio. The sensible heat flux H is then related to C_T through, for example, a relation of the form (Koshiek, 1982)

$$H = A C_T^{3/2}$$

Eq. 49

Where A is a constant, depending on temperature and boundary layer parameters. For dry lands the methods works fine since β is usually greater than 1.

4   Remote Sensing methods

It is difficult to classify Remote Sensing algorithms to estimate evapotranspiration (Kite and Droogers, 2000, Courault et al, 2005) since they range from empirical to completely deterministic, with no clear distinction between the different approaches. The complexity of the methods also greatly varies. The common denominator in most methods is that they allow spatially distributed estimates of ET and incorporate (parts of) the energy balance theory, the Monin-Obukhov similarity hypothesis and/or the flux profile relationships. Different examples of methods found in literature in increasing order of complexity and data needs are described below. The following (arbitrary) classification of methods is used:

- Thermal infra-red empirical methods
- Feedback approach
- Land parameterization and Remote Sensing
- Energy balance and similarity theory methods

4.1   Thermal infra-red empirical methods

This method assumes that it is possible to directly relate daily evapotranspiration (m) to the net radiation (W m^{-2}) and the instantaneous difference between surface and air temperature (K) according to the following relationship:

$$ET_d = Q^* + A - B(T_{surface} - T_{air})$$

Eq. 50

Where A and B are area specific constants. The methodology assumes that the soil heat flux is negligible when considering daily ET. It also assumes that the ratio of sensible heat flux and net radiation is constant throughout the day. Several authors have implemented this approach (Lagouarde, 1991, Seguin and Itier, 1983, Riou et al., 1998). Surface temperature as well as net radiation can be relatively straightforwardly derived from the spectral reflectance of the thermal and visible bands. The largest hurdle in the process is to acquire a reliable estimate of the air temperature. Two approaches are mentioned by Courault et al. (2005). One approach is to use geo-statistical interpolation methods of meteorological observations. Accuracy typically ranges from 20-30%. A second approach is to estimate T_a using empirical relationships with vegetation indices such as SAVI and NDVI.

4.2   Feedback approach

A number of authors have used the Penman-Monteith equation as basis to derive ET using Remote Sensing. Granger for example applies a modified version of the Penman-Monteith equation, which has been adapted to the unsaturated case and which uses vapour pressure deficit and net radiation as

inputs, to calculate actual evapotranspiration (ET_{act}) (Granger, 1989). Granger uses the relative evapotranspiration (ET_{rel}), which is defined as the ratio between actual and potential evapotranspiration, to account for non-saturated conditions. By establishing an empirical relationship between ET_{rel} and the drying power, which is defined as ET_{act} / (ET_{act} + Q^*), ET_{act} can be determined on the basis of net radiation, surface temperature, vapour deficit, and roughness heights without the necessity for prior estimates of the potential evapotranspitaion, air temperature and humidity. Granger (1995, 1997, 2000) uses the visible channels to calculate the surface albedo, which is used to calculate net radiation through:

$$Q^* = Q_{swn} + Q_{lwn}$$
<div align="right">*Eq. 51*</div>

Where Q^* (W m^{-2}) is the net radiation, Q_{swn} (W m^{-2}) is the net shortwave radiation and Q_{lwn} (W m^{-2}) is the net longwave radiation. The Q_{swn} is calculated by:

$$Q_{swn} = Q_{sw}(1 - \alpha)$$
<div align="right">*Eq. 52*</div>

Where α is the broad band surface albedo. Granger (1997) shows that AVHRR channel 2 albedo is a reasonable estimate of the broad band surface albedo. The net long wave radiation is usually estimated by measurements of temperature and humidity. Granger and Gray assume however that on clear days for dry continental atmospheres the net long wave radiation is proportional to the incoming shortwave radiation through:

$$Q_{lwn} = -4.25 - 0.24Q_{sw}$$
<div align="right">*Eq. 53*</div>

A salient characteristic of the methodology is that a feedback mechanism is implemented to directly estimate vapour pressure deficit. The mechanism states that the temperature and humidity in the air are a reflection of the portioning of energy at the earth's surface. Granger applies the converse and demonstrates that the observed surface temperature is a sufficiently accurate indicator of air humidity. Using field data the following empirical relation was derived for the daily vapour pressure deficit:

$$VP_{def} = -0.278 - 0.015T_{ltm} + 0.669VP^*_{TS}$$
<div align="right">*Eq. 54*</div>

Where VP_{def} (Pa) is the daily vapour pressure deficit, T_{ltm} (K) is the long term mean air temperature and VP^*_{TS} (Pa) is the saturation vapour pressure at the surface temperature.

To calculate the surface temperature Granger adopts a split window technique used by Prata and Platt (1991), which uses surface emissivities (ε) and brightness temperatures (T (K)) of AVHRR channels 4 and 5 respectively according to:

FutureWater Science for Solutions

$$T_s = 2.09 + (2.84T_4 / \varepsilon_4) - (2.03T_5 / \varepsilon_5)$$

<div align="right">*Eq. 55*</div>

The last variable for which spatial information is required is the surface roughness, needed to determine the aerodynamic resistance in the Penman-Monteith equation. Vegetation across basins usually varies considerably in type and height and therefore in roughness. Granger uses a linear relationship between the Normalized Difference Vegetation Index (NDVI) and surface roughness using known vegetation heights.

4.3   *Land parameterization and Remote Sensing*

Remote Sensing is also used commonly in combination with process based basin scale or agro-hydrological models to perform spatially explicit estimates of evapotranspiration.

Courault et. al. (2005) distinguish two types in this category; remote sensing forced models and assimilation of numerical models. Generally these models describe the exchanges between soil plant and atmosphere according to the physical processes occurring in each compartment with generally a fine time step (second, hour). Different complexity levels appear according to the process description: for example, if the vegetation and soil behavior are separated, then evaporation and transpiration are computed with a surface temperature for each part. Increasing levels of complexity require a higher degree of parameterization, which can (sometimes) be estimated by remote sensing data. A few examples are given below.

Choudhury and DiGirolamo (1998) for example use a biophysical model which links the water, energy and carbon processes by using satellite and ancillary data to quantify total evaporation, transpiration and biomass production (Choudhury, 1997). Transpiration is calculated using the Penman–Monteith equation in which the minimum canopy stomatal resistance is determined by the rate of carbon assimilation. Soil evaporation is computed as energy-limited and exfiltration limited. The rate of carbon assimilation, together with estimated respiration and soil water stress provides biomass production. Satellite observations are used to obtain fractional vegetation cover, surface albedo, incident solar and Photosynthetically Active Radiation (PAR), fractional cloud cover, air temperature, and vapour pressure. Precipitation is obtained by combining satellite and surface observations. Biophysical parameters of the model (e.g. soil hydraulic characteristics, and maximum carbon assimilation rate of a leaf) are determined from published records and land cover of the area.

4.4   *Energy balance and similarity theory methods*

4.4.1   **SEBAL**

The Surface Energy Balance Algorithm for Land (SEBAL) formulated by Bastiaanssen et al. (1998) is an image-processing model comprised of 25 computational steps that calculates the actual (ETact) and potential evapotranspiration rates (ETpot) as well as other energy exchanges between land and atmosphere. The key input data for SEBAL consists of spectral radiance in the visible, near-infrared and thermal infrared part of the spectrum. SEBAL computes a complete radiation and energy balance

along with the resistances for momentum, heat and water vapour transport for every individual pixel. The resistances are a function of state conditions such as soil water potential (and thus soil moisture), wind speed and air temperature and change from day-to-day.

Satellite radiances will be converted first into land surface characteristics such as surface albedo, leaf area index, vegetation index and surface temperature. These land surface characteristics can be derived from different types of satellites. First, an instantaneous evapotranspiration is computed, that is subsequently scaled up to 24 hours and longer periods.

In addition to satellite images, the SEBAL model requires the following routine weather data parameters:
- Wind speed
- Humidity
- Solar radiation
- Air Temperature

There is no data on land use, soil type or hydrological conditions required to apply SEBAL.

The primary basis for the SEBAL model is the surface energy balance. The instantaneous latent heat flux is calculated for each pixel of the image as a 'residual' of the surface energy budget equation:

$$L_v E = Q^* - G_0 - H$$ Eq. 56

Where LvE is the latent heat flux (W m-2), Q* is the net radiation flux at the surface (W/m2), G is the soil heat flux (W/m2), and H is the sensible heat flux to the air (W/m2).

The net radiation (Q*) is computed by subtracting all outgoing radiant fluxes from all incoming radiant fluxes according to

$$Q^* = Q_{s\downarrow} - \alpha Q_{s\downarrow} + Q_{L\downarrow} - Q_{L\uparrow} - (1 - \varepsilon_0)Q_{L\downarrow}$$ Eq. 57

Where Q_s is the incoming short-wave radiation (W/m2), α is the surface albedo (dimensionless), Q_L is the incoming long wave radiation (W/m2), Q_L is the outgoing long wave radiation (W/m2), and ε_o is the surface thermal emissivity (dimensionless). In Eq. 57, the amount of net short-wave radiation (Q_S - αQ_S) that remains available at the surface, is a function of the surface albedo (α). The broad band surface albedo α is derived from the narrow band spectral reflectances α (λ) measured by each satellite band. The incoming short-wave radiation (Q_S) is computed using the solar constant, the solar incidence angle, a relative earth-sun distance, and a computed broad band atmospheric transmissivity. This latter transmissivity can be estimated from sunshine duration or inferred from pyranometer measurements (if available). The incoming long wave radiation (Q_L) is computed using a modified Stefan-Boltzmann equation with an apparent emissivity that is coupled to the shortwave atmospheric transmissivity and a measured air temperature. Outgoing long wave radiation (Q_L) is computed using the Stefan-Boltzmann equation with a calculated surface emissivity and surface temperature. Surface temperatures are computed from the satellite measurements of thermal radiances.

FutureWater Science for Solutions

In Eq. 56, the soil heat flux (G_0) and sensible heat flux (H) are subtracted from the net radiation flux at the surface (Q^*) to compute the "residual" energy available for evapotranspiration (L_vE). Soil heat flux is empirically calculated as a G_0/Rn fraction using vegetation indices, surface temperature, and surface albedo. Sensible heat flux is computed using wind speed observations, estimated surface roughness, and surface to air temperature differences (ΔT) that are obtained through a sophisticated self-calibration between dry ($L_vE \approx 0$) and wet ($H \approx 0$) pixels. For the wet pixel it is assumed that $\Delta T = 0$. For the dry pixel ΔT is given by:

$$\Delta T = \frac{H r_{ah}}{\rho_{air} c_p}$$

Eq. 58

Where r_{ah} (s m^{-1}) is the near surface aerodynamic resistance to heat transfer, ρ_{air} (kg m^{-3}) is the moist air density and c_p (J kg^{-1}) is the specific heat at constant pressure. SEBAL solves this implicit equation iteratively. In first instance free convection is assumed, thereafter mixed convection is applied and buoyancy effects according the Monin-Obukhov similarity hypothesis are incorporated in the pixel dependent aerodynamic resistance to heat transfer. Empirically it has been shown that there is a linear relation between surface temperature (T_0) and ΔT. This relation is used to estimate ΔT for all pixels in the image.

The L_vE time integration is an interesting property of SEBAL. Knowing the instantaneous soil, latent and sensible heat fluxes makes it possible to calculate the evaporative fraction given by:

$$\Lambda = \frac{L_vE}{Q^* - G}$$

Eq. 59

The most important assumption of SEBAL is that the evaporative fraction is constant during the day. For periods longer than one day it may be assumed that the soil heat flux equals 0. The 24hr latent heat flux can therefore be determined by

$$L_vE_{24hr} = \Lambda Q^*_{24hr}$$

Eq. 60

The final step is to calculate monthly evapotranspiration data. This achieved by inserting L_vE_{24hr} into the Penman-Monteith equation (Eq. 36). Using this approach it is possible to inversely determine the surface resistance (r_s). Knowing the spatial distribution of the surface resistance makes it possible to calculate ET based on the Penman-Monteith equation and meteorological data for all days without satellite imagery.

4.4.2   SEBS and (S-)SEBI

The surface energy balance system (SEBS) is another semi-empirical process based method. The method is also based on the evaporative fraction in a manner similar to SEBAL. The method was first described by Menenti and Choudhury (1993). The concept was later included in a more comprehensive framework by Su (2002). A simplified method, called S-SEBI, which estimates surface fluxes from Remote Sensing was later further developed by Roerink et al. (2000). S-SEBI determines a reflectance

dependant maximum and minimum temperature for dry (T_H) and wet pixels (T_{LE}) and the evaporative fractions is determines as:

$$\Lambda = \frac{T_H - T_0}{T_H - T_{LE}}$$

The method assumes that at limiting cases at dry and wet pixels there is a linear relation between the maximum L_vE and H and surface reflectance (r_0). The method furthermore assumes that

$$T_H = a_H + b_H r_0$$

Eq. 62

$$T_{LE} = a_{LE} + b_{LE} r_0$$

Eq. 63

$$G_0 = f(NDVI, r_0)Q^*$$

Eq. 64

$$H = (1 - \Lambda)(Q^* - G_0)$$

Eq. 65

$$L_v E = \Lambda(Q^* - G_0)$$

Eq. 66

Because of the dependence on reflectance the major advantage of the method is that no additional meteorological data are required to determine the turbulent fluxes.

FutureWater Science for Solutions

5   Conclusions

The objective of the this project is to use spatial patterns of actual evapotranspiration in the calibration of hydrological models as opposed to more traditional methods which use hydrograph data only. The GO project therefore requires multi-temporal spatially explicit evapotranspiration across the study area. Remote Sensing is the only appropriate tool to generate these data. The point methods discussed in Chapter 3 are therefore not suitable.

The Remote Sensing methods discussed provide a range of options. The thermal infra-red method, although straightforward, is a purely empirical approach which depends on meteorological data and is therefore considered less suitable. The feedback approach described by Granger (1998) is a suitable methodology which can be applied across a number of sensors, is also physically based and relatively straightforward. The comprehensive energy balance methods such as SEBAL and SEBS are the most complete, but also the most complex methods. SEBAL has been applied in numerous projects across the globe and is therefore operationally more applicable.

Depending on the costs and complexity it is therefore proposed to apply either the feedback approach or SEBAL in this project to map the actual evapotranspiration in the Krishna basin.

6 References

Allen, R.G., Howell, T.A., Pruitt, W.O., Walter, I.A. and Jensen, M.E. (eds), 1991, Lysimeters for evapotranspiration and environmental measurements. ASCE, New York, USA, pp 444.

Allen, R., Pereira, L.A., Raes, D., Smith, M., 1998, Crop evapotranspiration; guidelines for computing crop water requirements, FAO Irrigation and Drainage Paper No. 56, FAO, Rome

Bastiaanssen, W.G.M., M. Menenti, R.A. Feddes and A.A.M. Holtslag, 1998. The Surface Energy Balance Algorithm for Land (SEBAL): Part 1 formulation, J. of Hydr. 212-213: 198-212

Bowen, I.S., 1926, The ratio of heat losses by conduction and by evaporation from any water surface, Phys. Rev., Springer Verlag, 383-414

Brutsaert, W. (1982) Evaporation into the atmosphere. D. Reidel Publishing Co., Dordrecht, The Netherlands, pp 300.

Choudhury, B.J., 1997. Estimating land surface evaporation using multispectral satellite and ancillary data. In: Kite, G.W., Pietroniro, A., Pultz, T. (Eds.), Applications of Remote Sensing in Hydrology, Proc. Symp. No 17, NHRI, Saskatoon, Canada.

Choudhury, B.J., 2000. Seasonal and interannual variations of total evaporation and their relations with precipitation, net radiation, and net carbon accumulation for the Gediz Basin area. J. Hydrol. 229 (1/2), 77–86.

Choudhury, B.J., DiGirolamo, N.E., 1998. A biophysical processbased estimate of global land surface evaporation using satellite and ancillary data. I. Model description and comparison with observations. J. Hydrol. 205, 164–185.

Courault, D., Seguin, B. and Olioso, A., 2005, Review on estimation of evapotranspiration from Remote Sensing data: From empirical to numerical modelling approaches, Irrigation and Drainage Systems, 19, 223-249

De Bruin, H.A.R., van den Hurk, B.J.J.M., Kohsiek, W., 1995. The scintillation method tested over a dry vineyard area. Boundary-Layer Meteorol. 76, 25–40.

Gieske, A., 2003, Operational solution for actual evapotranspiration, in: Understanding Water in a Dry Environment: Hydrological Processes in Arid and Semi-arid zones, ed. Simmers, I., Balkema Publishers, the Netherlands

Granger, R.J., 1989. Evaporation from natural nonsaturated surfaces. J. Hydrol. 111, 21–29.

Granger, R.J., Gray, D.M., 1990. A net radiation model for calculating daily snowmelt in open environments. Nordic Hydrol. 21, 217–234.

Granger, R.J., 1995. A feedback approach for the estimate of evapotranspiration using remotely-sensed data. In: Kite, G.W., Pietroniro, A., Pultz, T.J. (Eds.), Application of remote sensing in hydrology (Proceedings of the Second International Workshop, NHRI Symposium No. 14, Saskatoon, October 18–19, 1994, NHRI, pp. 211–222.

Granger, R.J., 1997. Comparison of surface and satellite-derived estimates of evapotranspiration using a feedback algorithm. In: Kite, G.W., Pietroniro, A., Pultz, T.J. (Eds.), Application of remote sensing in hydrology. Proceedings of the Third International Workshop, NHRI Symposium No. 17, October, 1996; NASA, Goddard Space Flight Center, Greenbelt, MD, NHRI, pp. 71–81.

Jackson, R.B., Carpenter, S.R., Dahm, C.N., McKnight, D.M., Naiman, R.J., Postel, S.L., and Running, S.W., 2001. Water in a changing world. Ecological Applications 11, 1027-1045.

Kite, G.W. and Droogers, P., 2000, Comparing evapotranspiration estimates from satellites, hydrological models and field data, Journal of Hydrology, 229, 3-18

Lagouarde, J.-P. 1991. Use of NOAA-AVHRR data combined with an agrometeorological model for evaporation mapping. International Journal of Remote Sensing 12: 1853–1864.

Menenti, M. and Choudhury, B.J. 1993. Parametrization of land surface evapotranspiration using a location dependent potential evapotranspiration and surface temperature range. In: Bolle H.J. et al. (Eds.), Exchange Processes at the Land Surface for a Range of Space and Time Scales, IAHS Publication. vol. 212, pp. 561–568.

Monin, A.S., and A.M. Obukov, 1954. Basic laws of turbulent mixing in the atmosphere near the ground. Tr. Akad. Nauk SSSR Geoph. Inst., No. 24(151), 1963-1987.

Monteith, J.L., 1965, Evaporation and environment, Sym. Soc. Exp. Biol., 19, 205-234

Penman, H.L., 1948, Natural evaporation from open water, bare soil and grass, Proc. Roy. Soc., A, 193, 120-146.

Prata, A.J., Platt, C.M.R., 1991. Land surface temperature measurements from the AVHRR, Proceedings of the Fifth AVHRR Data Users' Meeting. Tromso, Norway, 25–28 June 1991, pp. 433–438.

Riou, C., Itier, B. & Seguin, B. 1988. The influence of surface roughness on the simplified relationship between daily evaporation and surface temperature. International Journal of Remote Sensing 9(9): 1529–1533.

Roerink, G.J., Su, B. & Menenti, M. 2000. S-SEBI A simple remote sensing algorithm to estimate the surface energy balance. Physics Chim Earth (B) 25(2): 147–157.

Seguin, B. & Itier, B. 1983. Using midday surface temperature to estimate daily evaporation from satellite thermal IR data. International Journal of Remote Sensing 4: 371–383.

Su, Z. 2002. The surface energy balance system (SEBS) for estimation of turbulent heat fluxes. Hydrology and Earth System Sciences 6: 85–99.

Sugita, M. and Brutsaert, W. (1990) Regional surface fluxes from remotely sensed skin temperature and lower boundary layer measurements. Water Resources Research, 26, 2937-2944.

Verhoef, A., De Bruin, H.A.R., and Van den Hurk, B.J.J.M. (1997) Some practical notes on the parameter kB-1 for sparse vegetation. J. Appl. Meteor., 36, 560-572.